Article

Not peer-reviewed version

The Cultivation Modality and Barrier Maturity Modulate the Toxicity of Industrial Zinc Oxide and Titanium Dioxide Nanoparticles on Nasal, Buccal, Bronchial, and Alveolar Mucosa Cell-Derived Barrier Models

Helene Stuetz , Eva Ingeborg Reihs , Winfried Neuhaus , Maren Pflueger , Harald Hundsberger , Peter Ertl , Christian Resch , Gerald Bauer , Günter Povoden , Mario Rothbauer *

Posted Date: 25 January 2023

doi: 10.20944/preprints202301.0445.v1

Keywords: human mucosa models; nanotoxicology; titanium dioxide; zinc oxide; barrier health; barrier integrity

Article

The Cultivation Modality and Barrier Maturity Modulate the Toxicity of Industrial Zinc Oxide and Titanium Dioxide Nanoparticles on Nasal, Buccal, Bronchial, and Alveolar Mucosa Cell-Derived Barrier Models

Helene Stuetz [1,&], Eva I. Reihs [1,2,&], Winfried Neuhaus [3,4], Maren Pflüger [5], Harald Hundsberger [5], Peter Ertl [1], Christian Resch [6], Gerald Bauer [6,7], Guenter Povoden [7] and Mario Rothbauer [1,2,*]

[1] Faculty of Technical Chemistry, Institute of Applied Synthetic Chemistry and Institute of Chemical Technologies and Analytics, Vienna University of Technology, Getreidemarkt 9/163-164, 1060 Vienna, Austria
[2] Karl Chiari Lab for Orthopaedic Biology, Department of Orthopedics and Trauma Surgery, Medical University of Vienna, Währinger Gürtel 18-22, 1090 Vienna, Austria
[3] AIT Austrian Institute of Technology GmbH, Center Health and Bioresources, Competence Unit Molecular Diagnostics, Giefinggasse 4, Vienna, 1210 Austria
[4] Department of Medicine, Faculty of Medicine and Dentistry, Danube Private University, 3500 Krems, Austria
[5] Medical and Pharmaceutical Biotechnology, IMC University of Applied Sciences, Am Campus Krems, Trakt G, 3500 Krems an der Donau, Austria
[6] Science, Research and Development Division; Austrian Federal Ministry of Defence; 1090 Vienna, Austria
[7] CBRN-Defence-Centre, Austrian Armed Forces, 2100 Korneuburg, Austria
* Correspondence: mario.rothbauer@tuwien.ac.at
& Authors contributed equally.

Abstract: As common industrial by-products, airborne engineered nanomaterials are considered important environmental toxicants to monitor due to their potential health risks to humans and animals. The main uptake routes of airborne nanoparticles are nasal and/or oral inhalation, which are known to enable the transfer of nanomaterials into the blood stream resulting in rapid distribution in the body. Consequently, mucosal barriers present in nose, buccal and lung have been identified and intensively studied as the key tissue barrier to nanoparticle translocation. Despite decades of research, surprisingly little is known about the differences among various mucosa tissue types to tolerate nanoparticle exposures. One limitation in comparing nanotoxicological data sets can be linked to a lack of harmonization and standardization of cell-based assays, where a) different cultivation conditions such as air-liquid interface or submerged cultures, b) varying barrier maturity and c) diverse media substitutes have been used. The current comparative nanotoxicological study therefore aims at analyzing the toxic effects of nanomaterials on four human mucosa barrier models including nasal (RPMI2650), buccal (TR146), alveolar (A549), and bronchial (Calu-3) mucosal cell lines to better understand the modulating effects of tissue maturity, cultivation conditions and tissue type using standard Transwell cultivations at liquid-liquid and air-liquid interfaces. Overall, cell size, confluency, tight junction localization, and cell viability as well as barrier formation using 50% and 100% confluency was monitored using trans-epithelial-electrical resistance (TEER) measurements and Presto Blue assays of immature (e.g. 5 days) and mature (e.g. 22 days) cultures in the presence and absence of corticosteroids such as hydrocortisone. Results of our study show that cellular responses to increasing nanoparticle exposures are highly cell type specific, where bronchial mucosal cell barriers models cultivated under ALI conditions showed less tolerance to acute ZnO nanoparticle exposures. Additionally, stronger toxicities are found using early mucosa barriers compared to later barrier models being maturated under air-liquid cultivation conditions.

Keywords: human mucosa models; nanotoxicology; titanium dioxide; zinc oxide; barrier health; barrier integrity

 doi:10.20944/preprints202301.0445.v1

1. Introduction

A number of important global economic activities are attributed as sources of airborne nanoparticles (NPs) ranging from 1 to 100 nm in size including transportation pipelines, agricultural processes, fabric- and clothing manufacturing, metal- and construction industry as well as in food and health technologies. Airborne nanoparticles can either be generated intentionally as coatings for electronic component production, in medical, food and cosmetic applications or unintentionally as emissions during subtractive manufacturing processes and dissipation events. For any potentially toxic airborne nanomaterial, nasal and/or oral inhalation is the main route of entry. [1] After passing the nasal and oral cavities, aerosols travel through the pharynx, larynx and trachea reaching bronchi, bronchioles, and finally alveoli. The epithelial tissues that line the respiratory track include several different cell types that form specialized structures serving essential physiological functions such as blocking unwanted microorganism and small particles from tissue and blood stream penetration. [2] While nasal hair restrains particles ($\geq$ 1μm) from inhaled air, smaller particles can follow the respiratory system unstopped where they can interact with epithelial tissue surfaces that are unprotected by physical structures that promote air clearance and hinder particle entry. It is important to note that when NPs leave their route of purpose towards an uncontrolled environmental spreading their subsequent inhalation by living biological systems is generally considered dangerous and labelled as a potentially health hazard. [3] For instance, even advanced medical nanomaterials such as anti-bacterial coatings and nanodrug delivery systems in anti-cancer therapies or thermotherapies can exhibit significant toxic potentials following an unwanted intake. Here, dose- and site-of-entry dependent toxicity is strongly influenced by the intrinsic physicochemical properties of the nanomaterial such as material type, size, surface chemistry, and chemical inertness. [4] As one medical example, nanosilver exposure in a high dose can induce cytotoxic- and genotoxic effects, oxidative stress, cytokine secretion, and mitochondrial disruption caused by both particles as well as leaching ionic species. [5] In turn, inhalation of cerium oxide a prominent industrial process catalyst or other industrial by-products such as ultrafine carbon can result in a reduction of essential cellular and tissue physiological processes in the lung that can lead to strong inflammatory reactions. [6,7] Additionally, unintended inhalation of zinc oxide (ZnO) and titanium oxide (TiO_2), which are widely applied NPs for UV protection in sunscreens, cosmetic powders, electronics, and paints are known to provoke dermal toxicity, dysregulation of immune cells and potential toxicological effects in lung tissue due to airborne consumption. [8,9]

As an alternative to toxicological animal models, *in vitro* lung barrier systems exhibiting *in vivo-like* properties are often used to assess the health effects of airborne nanomaterials. [10,11] Due to their increased robustness, availability and assay reproducibility, lung epithelial cell lines are generally used in nanotoxicological studies instead of primary cells that exhibit only a limited lifespan. Nevertheless, optimization of cell culture conditions that promote cell viability, proliferation, and differentiation towards the formation of a tight barrier is key for conducting nanotoxicological screening including the application of an air-liquid-interface (ALI). [12] An ALI set-up is important since it closely reflects *in vivo* conditions of inhalation in the lower respiratory track where epithelial surfaces are covered by a thin liquid layer keeping the cells in a moist microenvironment. [13] This means that only an ALI system can properly simulate physiological-relevant toxicant or particle exposures. [11] A comparative study investigating submerged lung cell cultures in a liquid-liquid interface (LLI), with ALI culture of lung cells, and rat models demonstrated that ALI most closely represented the *in vivo* results following exposure to toxicants as indicated by similar cell viability and release of lung inflammation markers. [12] Additionally, ALI proved to be a very useful tool in toxicity and pharmacological studies of inhaled particles, revealing significant differences in secretion of pro-inflammatory IL-8 and oxidative stress to LLI upon ZnO nanoparticle exposure. [13] Furthermore, a platform capable of mimicking breathing motion including associated air flow and heating of the sample gas during exposure to adherent lung epithelial cultures was reported in an attempt to best emulate biotransformation of the exposed substances. [14] It is, however, important to note that in addition to optimum physiological-relevant culture conditions the

 doi:10.20944/preprints202301.0445.v1

choice of cell lines and applied bioactive compounds such as hormones are also critical in promoting reliable barrier formation.

To gain a deeper understanding of the complex interplay between cell culture conditions, media composition and cell types in nanotoxicological studies, four human tissue barrier models using nasal (RPMI2650), buccal (TR146), alveolar (A549), and bronchial (Calu-3) mucosal cell lines are in investigated using Transwell-based cultivation at liquid-liquid as well as air-liquid interface. Considering the entry route of airborne toxicants and there located as well as particle exposed respiratory epithelial tissues, a higher degree of in vivo-like properties can be reached by including differential epithelial cells lines deriving from first-contact tissues of the upper [15,16] (nasal and buccal) and lower [17,18] (bronchial and alveolar) respiratory tract. As the current study is part of a bigger project framework to develop a multi-mucosa on-a-chip system for nanoxoticological studies, the initial characterizations here were conducted with a shared medium formulation. Initially, cell size, confluency, tight junction localization, as well as barrier formation is monitored using trans-epithelial-electrical resistance (TEER) measurements throughout an incubation period of 22 days in the presence and absence of corticosteroids (e.g., dexamethasone or hydrocortisone). Furthermore, the impact of initial barrier confluency on nanomaterial dose-response behavior, the effect of initial 50% and 100% confluency in submerged cultures is evaluated over 24 h of nanomaterial exposure using Presto Blue viability assay. Finally, the effect of nanomaterial exposure is investigated using immature liquid-liquid mucosa barriers at day 5 and compared to the response of maturated mucosa barriers at day 22 cultivated under air-liquid interface conditions using TEER and Presto Blue assays. One intention of the current comparative study is the detailed characterization of the main mitigating factors known to influence nanotoxicological screening efforts, thus fostering better guidelines for improved harmonization and standardization of advanced *in vitro* cell based assays for inhalation studies.

2. Results

2.1. Initial characterization and seeding density optimization of the four mucosa cell lines

The first parameter to be investigated in any cell-based assays is concerned with optimizing seeding density needed to reliably establish 100% confluency for each cell type that leads to adequate barrier functionality and health. This aspect is of particular importance since inadequate seeding densities result in extended cultivation periods required to form healthy human barrier models featuring high barrier health and integrity. To study the growth characteristics of employed four mucosal epithelial cell lines, cell size and confluency, as well as doubling time of the four epithelial cell lines is initially investigated. Average cellular length was quantified using ImageJ microscopic image analysis, while the confluency was determined experimentally via cell counting and conducting cell titration experiments. As shown in Figure 1, microscopic evaluations highlight differences in cell sizes in the range of approx. 20 to over 200 µm exhibiting a characteristic polygonal epithelial cell morphology. As these significant differences in cell size between the individual tissue types impact the initial cell seeding density needed establish dense two-dimensional cell layers, the next set of experiments analyzed the effect of increasing initial cell seeding densities on barrier confluency.

Preprints (www.preprints.org) | NOT PEER-REVIEWED | Posted: 25 January 2023 doi:10.20944/preprints202301.0445.v1

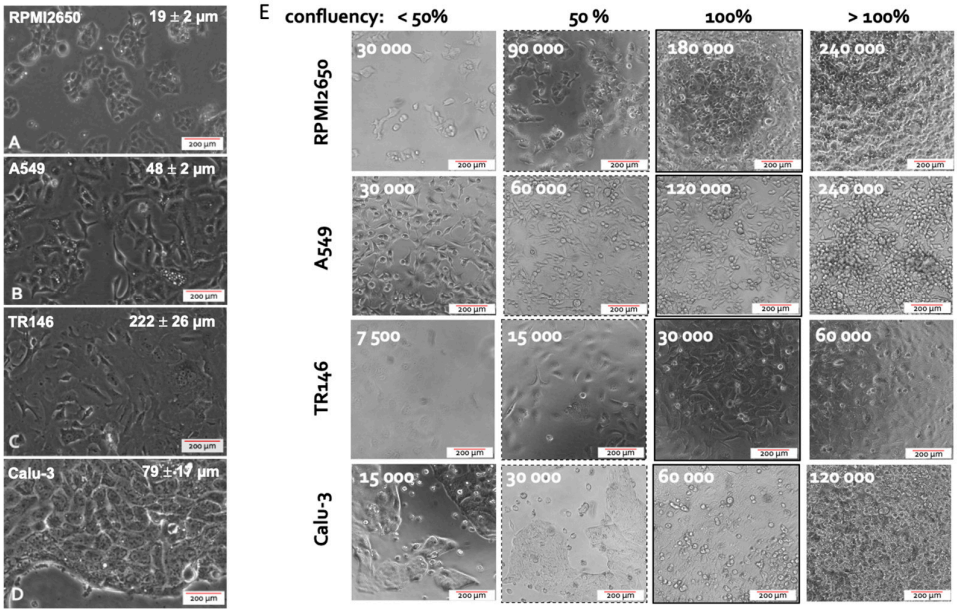

Figure 1. (A–D) Representative phase contrast images of cell morphology the four different mucosa cell lines including (A) RPMI2650 (B) A549 (C) TR146 and (D) Calu-3 grown in 75 cm^2 cell culture flasks. (E) Representative phase contrast images of the four epithelial mucosal cell lines at various monolayer confluency resulting from variations of initial cell seeding densities 24 h post seeding in cell culture-treated 96-well plate format with a total growth area of 0.33 cm^2.

As shown in Figure 1A, RPMI2650 epithelial cells derived from squamous cell carcinoma of the nasal mucosa showed a tendency to grow in small patches. The very small ovoid to squamous appearing cells displayed an average size of 19.3 ± 2.3 µm reaching confluency of approximately 95% at an initial cell seeding density of 6 *10^5 cells/cm In turn, A549 cells, which are epithelial cells of an adenocarcinoma of the alveolar lung epithelium, revealed a characteristic spindle-like morphology when seeded below confluency with an average size of 47.4 ± 5.2 µm. Growing in bigger patches this alveolar cell type reached confluency at an initial seeding density of 4*10^5 cells/cm Interestingly, TR146, a squamous cell carcinoma cell line of the buccal epithelium displayed the biggest cell size of 222.3 ± 25.9 µm producing cell monolayers when seeded at approximately 1*10^5 cells/cm^2; while Calu-3 being a bronchial adenocarcinoma cell line displayed an average size of 79.1 ± 16.6 µm with confluency at a seeding density of 1.8*10^5 cell/cm Summarizing the performance indicators in Table 1, the optimized initial cell seeding densities were used in all subsequent experiments in microtiter plates as well as Transwell insert approaches to provide each individual cell type the best starting conditions to form tight human cell barriers taking significant cell-specific variations in both cell size as well as growth capacities into account.

Table Summary of fundamental characteristics of the four mucosa cell lines including cell length, cell density of a confluent monolayer as well as mean doubling time.

Cell Line	Cell Length [µm, mean ± sdev]	Confluency [cells/cm^2]	Doubling time [h]
RPMI2650	19.3 ± 2.3	6 *10^5	41.2 ± 9.3
A549	47.4 ± 5.2	4 *10^5	34.6 ± 9.0
TR146	222.3 ± 25.9	1 *10^5	63.8 ± 17.7
Calu-3	79.1 ± 16.6	1.8 *10^5	137.3 ± 20.4

 doi:10.20944/preprints202301.0445.v1

2.2. Optimization of liquid-liquid interface (LLI)-based cultivation approach and transfer to air-liquid interface (ALI) cultivation of human mucosa barrier models

As a next step, the initially optimized protocols for establishment of tight monolayers of the four individual cell lines were transferred and reevaluated for liquid-liquid (LLI) as well as air-liquid (ALI) interface cultivation approaches. Both methods benefit from using a porous membrane as cultivation surface for epithelial barrier cell growth, where the separation into apical and baso-lateral cell culture compartment allows for cell polarization that more closely mimics the physiological properties. The additional introduction of an air-liquid interface further induces cell differentiation and barrier maturation. To monitor barrier formation in more detail, in the next set of experiments trans-epithelial electrical resistance (TEER) monitoring was performed as non-invasive in situ approach to evaluate barrier integrity as it efficiently detects tight junction formation dynamics in the presence and absence of corticosteroid additives as well as ALI. First, barrier maturation was investigated at the LLI, where medium is supplied in the basal as well as apical compartment. To increase tight junction formation thus barrier maturation capacity, hydrocortisone was supplied to the complete medium at an effective concentration of 1 μM with TEER recordings being performed over a total cultivation duration of 22 days on collagen I-coated Transwell inserts. Data of Figure 2 confirms that barrier maturity and integrity improved over time for both treated and untreated barrier models of any cell type ($p<0.05$; two-way ANOVA with mixed effects analysis test). During the first 8 days of cultivation, corticosteroid treatment only showed slightly increased barrier maturation capacities ($p>0.05$), with overall barrier formation boosted only for Calu-3 barrier models when treated with hydrocortisone compared to the respective untreated controls ($p<0.005$). The least improvement in barrier maturation by supplementation with hydrocortisone was observable for RPMI2650 (Figure 2A), followed by A549 and TR146 which all together showed no TEER improvement ($p>0.05$). Notably, the bronchial barrier model established with Calu-3 cells was affected by hydrocortisone treatment and improved overall TEER values after 8 days of cultivation at the LLI resulting in an overall increase of TEER from 173.5 ± 11.1 Ω*cm² to 270.4 ± 32.4 Ω*cm² within 8 days ($p<0.005$). Even though in earlier time points the barrier maturation was faster for the hydrocortisone treated Calu-3 barriers, both treated and untreated Calu-3 cells reached comparable final TEER values after 22 days in LLI conditions.

Preprints (www.preprints.org) | NOT PEER-REVIEWED | Posted: 25 January 2023 doi:10.20944/preprints202301.0445.v1

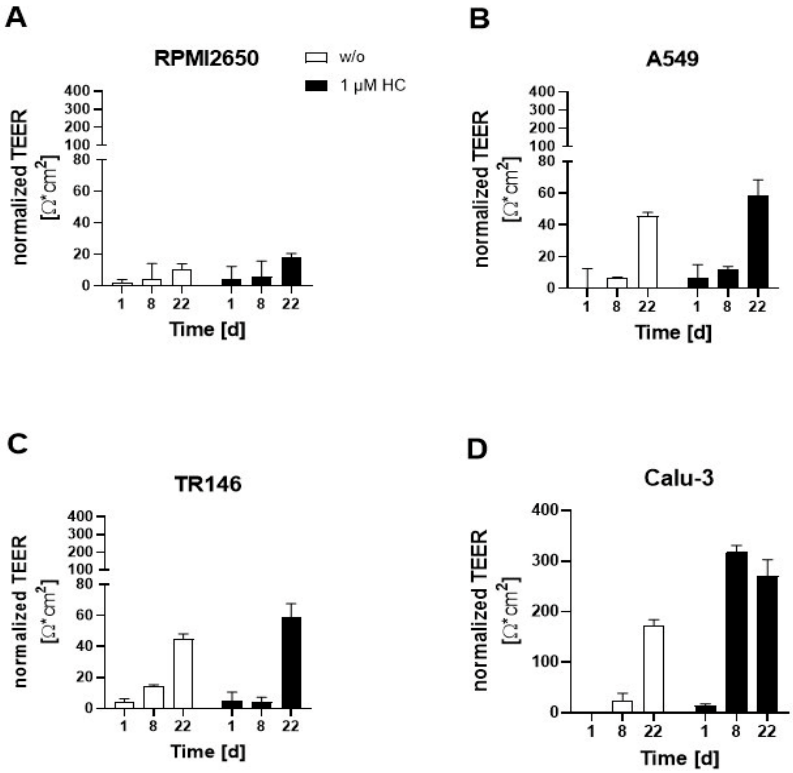

Figure 2. Effect of hydrocortisone (HC) on TEER-based read-out of barrier maturation dynamics of mucosa cells grown at confluency on porous membrane inserts throughout 22 days of liquid-liquid interface (LLI) culture for (A) RPMI2650, (B) A549, (C) TR146, and (D) Calu-Data is expressed as mean ± standard deviation for n=3 replicates.

Next the impact of ALI conditions on maturation capacities of human barrier model [156,188,195] was investigated using a similar setup as the above corticosteroid experiments. To determine whether an ALI boosts barrier functionality the apical medium was removed after 8 days of submerged cultivation duration to allow the cell layers to continue to be grown at ALI conditions with baso-lateral medium exchange every other day for another 14 days. As a side note, for successful establishment of ALI conditions, some optimizations in total volume of the basal medium compartment were necessary by switching from conventional Costar™ microtiter plates to more specialized Thincert® plates, where 4 mL of basal medium could be supplied at ALI conditions to provide a comparable amount of total medium to provide similar nutrient supply frequencies of every other day with regard to the optimized LLI cultivation protocols used in prior Transwell experiments. As indicated in Figure 3A, TEER values of nasal RPMI2650 barrier models improved from 10.8 ± 3.2 Ω * cm² at LLI to ALI: 14.8 ± 6.0 Ω * cm² for ALI-based barrier maturation protocols with further improvement for the 1 µM hydrocortisone treatment boosting TEER values up to 33.2 ± 1.7 Ω * cm² at ALI at day 22 post-seeding. In contrast, for the alveolar A549 barrier model shown in Figure 3B, the LLI tended to generally show higher TEER values (LLI: 45.5 ± 2.4 Ω * cm², and ALI: 21.6 ± 8.1 Ω * cm²). Hydrocortisone treatment was effectively boosting TEER for both cultivation protocols and approximated both techniques to 58.7 ± 9.6 Ω * cm² at LLI and 51.5 ± 1.1 Ω * cm² at ALI. Similarly, TR146 also showed increased barrier integrity when cultured at LLI as shown in Figure 3C ($p<0.05$; two-way ANOVA with multiple comparisons test) yielding TEER values of 44.8 ± 3.2 Ω * cm² for LLI compared to 33.0 ± 6.7 Ω * cm² for ALI conditions. Also, TR146 barriers were unaffected by hydrocortisone for the ALI culture technique (27.8 ± 0.9 Ω * cm²). Again, alveolar Calu-3 barriers showed by far the highest barrier integrity, with 173.5 ± 11.1 Ω * cm² for LLI and 101.4 ± 3.7 Ω * cm² for ALI as shown in Figure 3D ($p<0.0001$). Moreover, hydrocortisone treatment boosted barrier maturation significantly up to final TEER values of 270.4 ± 32.5 Ω * cm² and to 491.3 ± 25.7 Ω * cm² for

Preprints (www.preprints.org) | NOT PEER-REVIEWED | Posted: 25 January 2023 doi:10.20944/preprints202301.0445.v1

LLI and ALI, respectively. For the sake of comparability in all subsequent experiments 1 µM hydrocortisone (HC) was added to all mucosa cell models.

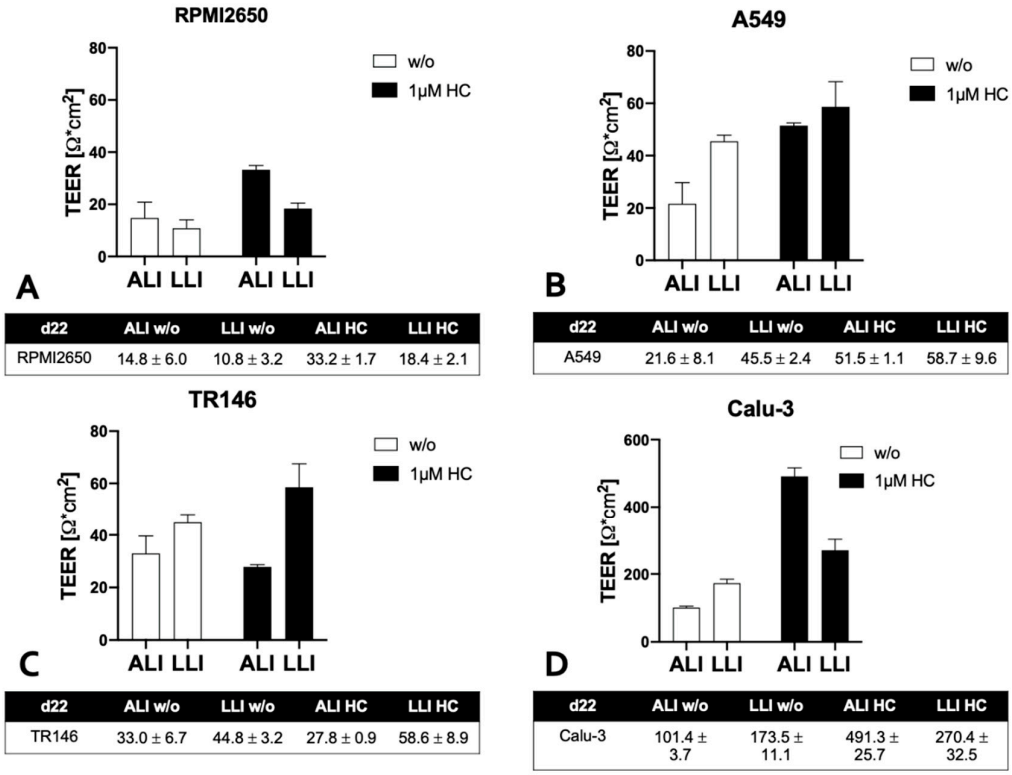

d22	ALI w/o	LLI w/o	ALI HC	LLI HC
RPMI2650	14.8 ± 6.0	10.8 ± 3.2	33.2 ± 1.7	18.4 ± 2.1

d22	ALI w/o	LLI w/o	ALI HC	LLI HC
A549	21.6 ± 8.1	45.5 ± 2.4	51.5 ± 1.1	58.7 ± 9.6

d22	ALI w/o	LLI w/o	ALI HC	LLI HC
TR146	33.0 ± 6.7	44.8 ± 3.2	27.8 ± 0.9	58.6 ± 8.9

d22	ALI w/o	LLI w/o	ALI HC	LLI HC
Calu-3	101.4 ± 3.7	173.5 ± 11.1	491.3 ± 25.7	270.4 ± 32.5

Figure 3. Impact of air-liquid (ALI) compared to LLI cultivation on TEER in the presence and absence of hydrocortisone. Cells were grown on porous membrane inserts for 22 days with initial LLI cultivation period of 8 days followed by 14 days of barrier maturation at the ALI in the presence and absence of hydrocortisone (HC). Data is expressed as mean ± standard deviation for n=3 replicates.

2.3. Impact of barrier cell confluency on the dose response readout of human barrier models exposed to TiO_2 and ZnO nanoparticles

Following the establishment of optimum seeding density on barrier maturation for each of the four mucosal cell lines in the first section, the following investigations focused on the dose-time responses of lung, nasal and buccal cell barrier models using two well established nanoparticle types. The four barrier cell models were plated at 50% and 100% confluency and incubated for different exposure times up to 24 h in the presence of increasing concentrations of ZnO and TiO_2 nanoparticle solutions. Cell viability was determined after 1, 4, and 24 hours using the PrestoBlue™ viability assay. Figure 4 shows the effect of ZnO nanoparticles for each individual cell line using an immature state at 50% confluency. A general trend was observable, where incubation times of 4 h already resulted in compromised cell viability at high concentrations above 1mM for ZnO nanoparticle exposure. Moreover, longer incubation times of 24 h enhanced this initial cytotoxic response, and showed cell viability decreased significantly starting from 0.5 mM ZnO-NPs. For RPMI2650, the cell viability declined to 74 ± 1.7% at 1 mM and to 73 ± 1.8% at 2 mM ZnO-NPs at 4h. At 24 h cell viability was compromised to 68 ± 6.2% at concentrations of 0.5 mM, 38 ± 0.4% at 1 mM and 26 ± 2.6% at 2 mM (Figure 4A). For A549, a slight increase in cell viability was observed at 1 h incubation indicating most probably an initial stress response. After 4h, the cell viability dropped to 90 ± 1.0% at 1 mM and 85 ± 0.6% at 2 mM, which was further exacerbated within 24 h the cell viability further dropped to 87 ± 2.5% at 0.5 mM, 58 ± 4.2% at 1mM and 49 ± 3.6% at 2 mM (Figure 4B). For TR146 the incubation period of 1h, already showed a cytotoxic effect of 84 ± 1.4% at 0.5 mM, 71 ± 3.6% at 1 mM and 73 ± 2.2% at 2

Preprints (www.preprints.org) | NOT PEER-REVIEWED | Posted: 25 January 2023 doi:10.20944/preprints202301.0445.v1

mM, which intensified in longer incubation times. For 4h cell viabilities of 68 ± 1.3% at 0.5mM, 59 ± 1.3% at 1mM and 59 ± 2.0% at 2 mM were determined. After 24 h cell viability was further decreased to 12 ± 0.7% at 0.5mM, 5 ± 0.8% at 1mM and 6 ± 0.7% at 2 mM (see Figure 4C). Interestingly, the bronchial barrier Calu-3 model showed lowest susceptibility towards ZnO-based toxic events with a slight increase in cell viability after 1h for concentrations higher than 0.5 mM (Figure 4D), 107.6 ± 3.3% for 2 mM, 107.9 ± 5.1% for 1 mM, and 107.6 ± 2.6% for 0.5 mM. In contrast to the three other immature barrier models, this trend was continued at 4h post-incubation (2 mM: 113.6 ± 3.9% and 1 mM: 107.3 ± 3.0% viability). However, after 24 h of ZnO nanoparticle exposure cell viability for concentrations above 1 mM started to decline (2 mM: 93.9 ± 4.21% and 1 mM: 91.96 ± 0.28% viability), while the slight increase in cell viability at lower concentrations again may be attributed to cell stress rather than cytotoxic events.

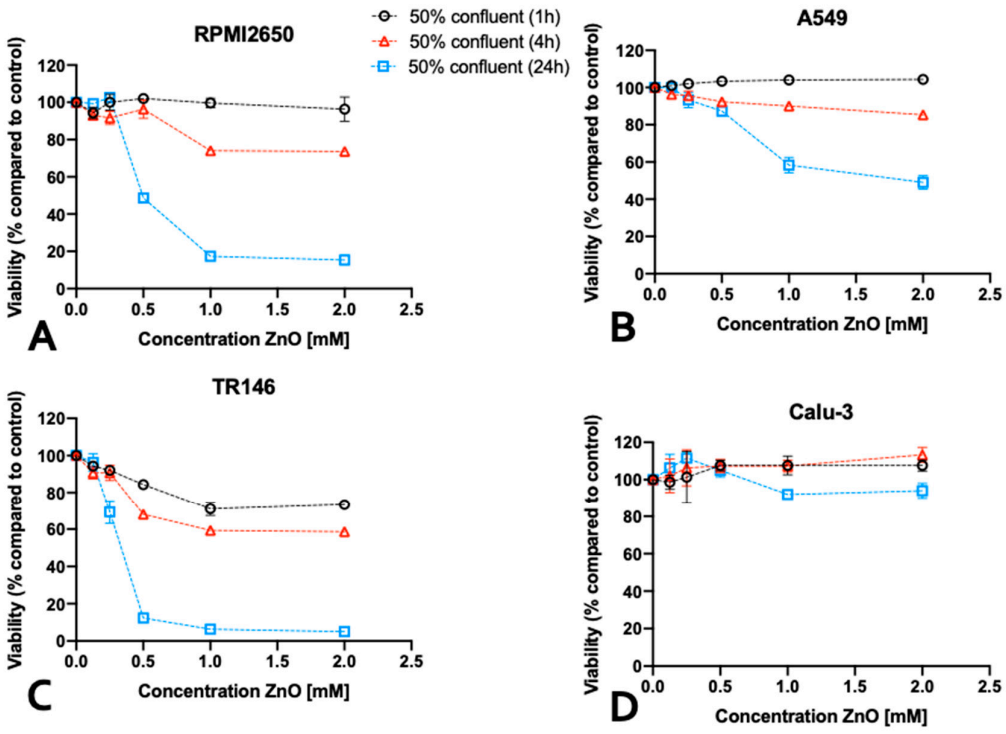

Figure 4. ZnO nanoparticle toxicity of immature barrier cell monolayers in conventional cell culture-treated microtiter plates at 50% cell confluency using a Presto Blue assay at 1, 4 and 24 h post exposure to 70-90 nm sized, uncoated ZnO-NPs for (A) RPMI2650 (B) A549 (C) TR146 and (D) Calu-Data is expressed as mean ± standard deviation for n=3 replicates.

In contrast to ZnO nanoparticles, which were selected for the well-reported cytotoxic effects of both zinc oxide particles as well as secreted zinc ions, TiO_2 nanoparticles did not negatively affect the viability of the immature cell models (see Figure 5). For RPMI2650, a slight increase in cell viability was observed in the samples treated for 24 h with TiO_2 nanoparticles. An increase in viability was also observed for TR146, after 1 h treatment, whereas for 2 mM TiO_2 nanoparticles cell viability of 117 ± 10% was observed. For A549 and Calu-3 neither up- now downward change in cell viability was observed independent of concentrations throughout the entire 24 h incubation period with TiO2-NPs.

Preprints (www.preprints.org) | NOT PEER-REVIEWED | Posted: 25 January 2023 doi:10.20944/preprints202301.0445.v1

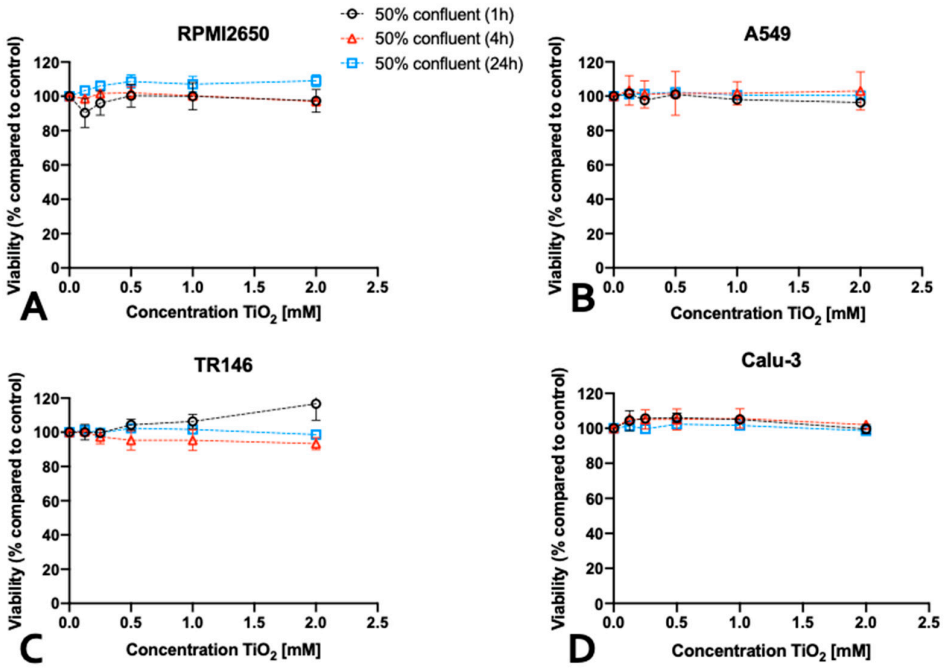

Figure 5. TiO2 nanoparticle toxicity in submerged cultures at 50% confluency. Cell viability was measured using a Presto Blue assay at 1, 4 and 24 h post exposure to 5-6 nm sized, uncoated TiO2-NPs. (A) RPMI2650 (B) A549 (C) TR146 and (D) Calu-Data is expressed as mean ± standard deviation for n=3 replicates. Two-way ANOVA with Tukey post-hoc test. ($p < 0.0332$ (*), $p < 0.0021$ (***), $p < 0.0002$ (***), $p < 0.0001$ (****)).

It has to be noted that most investigations of nanoparticle toxicity in conventional studies have been performed for a variety of cell lines seeded frequently at sub-confluent levels, thus making a comprehensive evaluations based on published data on the effect of barrier maturation stages almost impossible. Consequently, the impact of barrier maturity on cytotoxicity was investigated in more detail in the next set of experiments, by exposing mucosal cell lines established at 50% or 100% confluency with both nanoparticle types for up to 24 h. As shown in Figure 6, significant differences in the cytotoxic response upon ZnO-NP treatment was observed only with incubation times of 4 and 24 h and in the presence of concentrations of 2 mM ZnO-NPs and 1 mM ZnO-NPs. For RPMI2650 (Figure 6A) this difference was significant for 4h, with 1.14 ± 0.02-fold higher cytotoxicity in 50% confluency ($p<0.0002$) and a 1.70 ± 0.16-fold higher cytotoxicity after 24 h ($p<0.0001$). Furthermore, a similar picture was seen for A549 (Figure 6C), where after 4h incubation time a 15% increase in cytotoxic effect was observed ($p<0.0001$), whereas for 24 h a 1.37 ± 0.07 times higher effect was observed in cultures of 50% confluency ($p<0.0001$). Contrarily, TR146 show a different trend (Figure 6E). A significant difference in cytotoxicity between 50% and 100% coverage of growth area, was only observed after 4h of incubation time, with a change of 16% ($p<0.02$). For Calu-3 (Figure 6G), no significant difference ($p>0.1$) in cytotoxicity could be observed in correlation with the confluency (2 mM: 1.02 ± 0.04-fold higher in 50% confluent culture after 4h and 1.04 ± 0.03 after 24 h). A similar trend was observed for the 0.25 mM concentration, with a 1.11 ± 0.09-fold higher cytotoxicity in 50% confluent culture after 4 h ($p>0.31$) and was lower after 24 h (0.95 ± 0.01-fold; $p>0.1$). For TiO_2 nanoparticles, no significant difference in cytotoxicity for any of the four mucosal cell lines was observed in dependence of confluency (Figure 6 B,D,F,H).

Preprints (www.preprints.org) | NOT PEER-REVIEWED | Posted: 25 January 2023 doi:10.20944/preprints202301.0445.v1

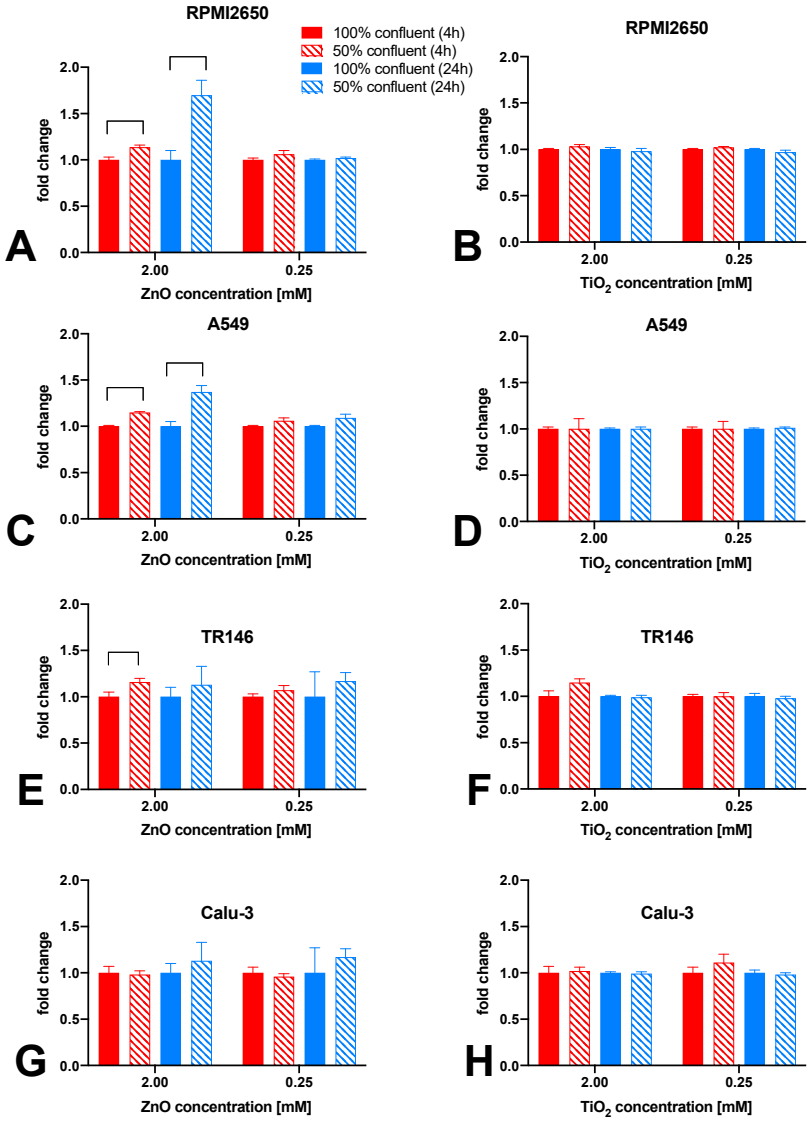

Figure 6. The impact of cell confluency on nanoparticle cytotoxicity of four mucosal cell lines including (A, B) RPMI2650, (C, D) A549, (D, E) TR146, and (F,G) Calu-Cell viability was measured using a Presto Blue assay at 4 and 24 h post-exposure to 80 nm sized, uncoated ZnO-NPs (A, C, E, G) as well as 5nm sized, uncoated TiO2-NPs (B, D, F, H). Data is expressed as mean ± standard deviation for n=3 replicates. Two-way ANOVA corrected with a Tukey test: $p < 0.0332$ (*), $p < 0.0021$ (**), $p < 0.0002$ (***), $p < 0.0001$ (****).

2.4. Toxicological evaluation of mature mucosa barrier models challenged with subtoxic and toxic ZnO and TiO_2 nanoparticle concentrations

To further investigate the modulating effects of tissue microphysiology on barrier integrity, the four mucosa barrier models cultivated using the optimized ALI protocols were treated with ZnO or TiO2 nanoparticle solutions. In a comparative study mucosa barrier toxicity data were collected using ALI and submerged monolayer cultures throughout 24 hours of exposure to ZnO and TiO_2 nanoparticles. In Figure 7 viability results of submerged cultures (100% confluency in cell culture-treated microtiter plates) are compiled using viability and TEER readouts. As shown in Figure 7A and Figure S1A, cytotoxicity of 2 mM ZnO NPs was highest in RPMI2650 barriers including submerged cultures (26.0 ± 2.6% viability) and mature barrier models (74.0 ± 8.8% viability). For the

 doi:10.20944/preprints202301.0445.v1

lower exposure concentration of 0.25 mM, ZnO NPs showed a stress response in submerged cultures (104.3 ± 0.6% viability) which was not observable for mature barrier models higher toxicity in the barrier models (91.5 ± 3.0% viability). TiO_2 exposure showed a similar stress responsiveness of the conventional 2D monolayer model for a 2 mM concentration (submerged: 107.0 ± 1.7% viability vs. mature: 87.9 ± 11.9% viability) as well as the 0.25 mM nanoparticle concentration (submerged: 103.3 ± 0.6% viability vs. mature: 91.4 ± 10.0% viability). Overall, both TiO_2 and ZnO showed an initial decline in barrier integrity ($p<0.005$) followed by a string increase of TEER ($p<0.0001$) relative to non-exposed control. Figure 7B and Figure S1B indicate, that A549 cultures show the lowest viability in submerged cultures treated with 2 mM ZnO NPs (67.3 ± 3.1% viability compared to mature barrier (82.1 ± 12.0%). For 0.25 mM ZnO NPs, RPMI2650 cultivated under submerged and ALI conditions showed no toxicities with 102.7 ± 0.6% viability vs. 91.3 ± 6.9% for submerged and ALI samples ($p>0.05$). A similar trend was observed for both TiO_2 nanoparticle exposure scenarios: The 2 mM concentration exposure resulted in a viability of 100.3 ± 0.6% in submerged cultures and 104.2 ± 9.3% in the mature barrier model. At a 0.25 mM TiO_2 concentration, viabilities of 102.7 ± 0.6% in submerged cultures versus 108.4 ± 7.7% for the mature barrier model were observable. Figure 7C and Figure S1C further confirm the overall lower cytotoxic response of mature barriers also for the TR146 cell model, where the submerged cells resulted in a viability of 5.7 ± 0.6% after 24 h incubation with 2 mM ZnO while the mature barrier demonstrated a viability decline to 73.1 ±26.8% ($p<0.0001$). TiO_2 NP exposure resulted in a slight trend for viability increase for mature barrier models (106.1 ± 14.1% for 2 mM and 106.1 ± 14.1% for 0.25 mM). Even though the viability read-out for 2 mM ZnO nanoparticles indicated cell death, the barrier integrity analyzed by TEER was unaffected ($p>0.05$). In contrast to the first three mucosa barrier models, Calu-3 cells showed responses similar to the 2D mono cultivation approach analyzed before again a quite different response (see Figure 7D and Figure S1D). As shown in SI Figure 1D, cell viability was more affected in the mature barrier model, than in the submerged culture with 95.3 ± 0.6% at 2 mM ZnO for submerged monolayers vs. 55.5 ± 21% for mature barrier ($p<0.05$). This was also reflected in a significant decline of TEER values by 30% over 24 h of exposure ($p<0.01$) found with the ALI conditions. Matured Calu-3 barriers showed no significant decline of cell viability in the range of 77.4 ± 15.1% and 82.8 ± 27.0% when exposed to 2 mM and 0.25 mM TiO_2 nanoparticles ($p>0.1$), respectively. Nonetheless, this stress response that after 1 hour of exposure resulted in TEER increase by 20% that again levelled off around 90% of the initial resistance values ($p>0.05$) after 24 h or exposure indicating most probably barrier regeneration processes.

Preprints (www.preprints.org) | NOT PEER-REVIEWED | Posted: 25 January 2023 doi:10.20944/preprints202301.0445.v1

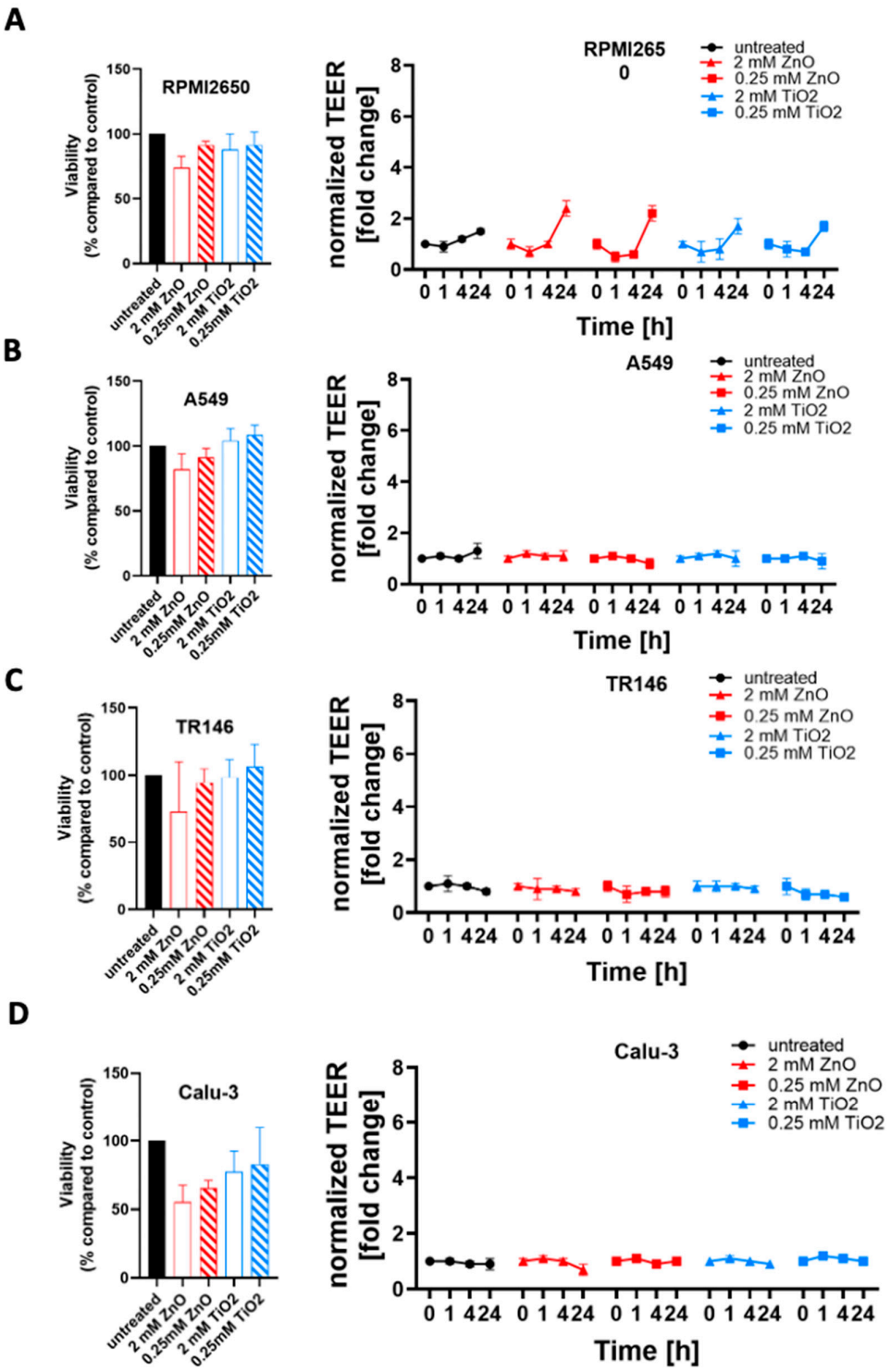

Figure 7. Comparison of zinc oxide and titanium dioxide nanoparticle toxicity in dependence of culture technique. Cell viability was measured after 24 h incubation with nanoparticles, measured using a Presto Blue Assay, (A) RPMI2650, (B) A549, (C) TR146, and (D) Calu-Data is expressed as mean ± standard deviation for n=3 replicates. Two-way ANOVA with Tukey post-hoc multi-comparisons test.

 doi:10.20944/preprints202301.0445.v1

3. Discussion & Prospects

The human airway is exposed to thousands of liters of air and therefore to a multitude of toxicants on a daily basis. Airborne nanomaterials, such as ZnO and TiO_2 nanoparticles are formed as a side product of many industrial processes and are known to increasing over time due to accumulation in the environment. [4] The investigation of nanomaterial-biology interactions and the potentially toxic effects on human barriers are of high importance to understand their impact on human health. The current work focused on the establishment of four airway mucosal cell lines (nasal, buccal, alveolar, and bronchial epithelium) as mature barrier models at the air-liquid interface for acute toxicological evaluation of nanoparticles under physiologically more relevant culture conditions. ZnO and TiO_2 nanoparticle toxicity was compared within multiple culture conditions and techniques. Additionally, the beneficial effect of hydrocortisone which has previously been reported to support barrier integrity by aiding the assembly process of ZO-1 to other proteins of the junction complex, [19] which in turn boosts barrier resistances investigated by TEER. To successfully optimize a set of four mucosa barrier models for nanotoxicological studies, firstly cell characteristics, such as growth conditions, doubling time, size of cells, and corresponding confluency conditions were evaluated and matched to those found in literature as well as general information provided by cell supplies (i.e., the ATCC). The use of RPMI2650 cells as a valid nasal mucosa barrier model was demonstrated previously in other studies, showing excellent application potential, and justifying the choice for this specific cell line. [20] A similar reasoning stands for TR146, a buccal mucosa cell line that was previously optimized to be used as a barrier model at the air-liquid interface by Lin et al., thus presenting a valid barrier model of the oral mucosa. [21] The choice of A549 as a barrier model for toxicity testing may seem unpopular at first, given the many reported limited barrier formation properties of A549. [22] However, provided the high frequency of applications in toxicological screening, this cell line represents a well-established model for human alveolar epithelium that can be used for cross-study comparisons. [7,23–26] In turn, the Calu-3 cells is a more obvious choice as a barrier model for the bronchial mucosa due to their excellent barrier maturation and tight junction formation properties. [27–30] Notably, Calu-3 cells have also been reported previously to form more physiological barrier models of the lung epithelium in comparison to other bronchial epithelial cell lines such as NHBE or NL-20. [31]

Barrier integrity results measured in TEER values of this study showed that RPMI2650 barriers exhibited TEER values that are close to those of excised nasal mucosa samples, [32,33] and are also comparable with TEER values reported in previous studies. [34] In accordance with previous studies TR146 cells formed stronger barriers at LLI compared to ALI. [35,36] Calu-3 further outperformed the other three mucosal cell lines in terms of barrier maturation potential yielding highest TEER values when cultivated under ALI conditions at comparable orders of magnitude reported previously. [27,37] Barosova et al. already discussed that TEER values at LLI as well as ALI protocols are subject to high inter-laboratory variability, [38] which can attribute to the observed lower TEER values. Notably, we decided for the current study to use a common media supplement formulation not only for the work conducted in this subproject, but also as collective starting point for potential simultaneous on-chip co-cultivation. Further optimizations of media conditions and supplements, as well as harmonization of individual ALI protocols are currently under investigation in the next project phase of on-chip integration to optimize the individual barrier properties.

Building from the aspect of barrier formation, the effect of different culture conditions on the toxicity of applied ZnO and TiO_2 nanoparticles were investigated. Notably, in our study confluency and maturity significantly affected the cytotoxic profile of ZnO nanoparticles in three out of the four mucosal cell lines. As discussed by Heng et al. there are two major factors influencing nanoparticle toxicity in submerged cell culture including firstly, the nanoparticle per cell ratio and secondly the nanoparticle to culture surface area ratio. [39] Even though the fact that individual cell within a confluent monolayer can potentially be less exposed to nanoparticles and that junctions in between cells, secreted cytokines, and growth factors could also dampen the cytotoxic effect, in our current study both nanoparticle diameters below 100 nm were selected to allow active as well as passive

 doi:10.20944/preprints202301.0445.v1

nanomaterial uptake, which makes transport inhibition phenomenon over a course of 24 h very unlikely.

Overall, when comparing submerged toxicity data of frequently used sub-confluent cells and Transwell barrier model toxicity responses are challenging because barrier models are more often used for material transport studies than detailed nanotoxicology studies. Even though both constitute viable and well-established models, in our opinion future studies must investigate a variety of human mucosa models in more comprehensive comparative studies, as highlighted by our current study, using more physiological approaches such as ALI protocols. As demonstrated by Leroux et al. air-liquid interface compared to submerged cultures more closely mimics gene expression levels upon TiO_2 nanoparticle exposure to that *in vivo*. [40,41] Here, Calu-3 cells showed the least cytotoxic effects upon ZnO exposure, which aligns well with comparable other studies of submerged cultures. [42] Most importantly, the type of barrier cell severely affected the nanotoxicological results in the current study. For instance, when comparing cell specific results using the optimized ALI culture protocols in the current study Calu-3 bronchial barriers showed a less tolerance to zinc oxide nanoparticles compared to established buccal, nasal and alveolar models. We could highlight the importance of barrier cultivation state when conducting toxicological nanoparticle studies interfacing human tissue models. Furthermore, conducting such studies under defined and comparable cultivation conditions as demonstrated here, for multiple tissue models allows for potential future harmonization on how to reproducibly perform nanomaterial interaction studies with higher lab-to-lab comparability in tissue-specific analyses.

For future nanotoxicological studies on the established multi-mucosa barrier models, the next advancement needs to integrate dynamic culture conditions using microfluidic organ-on-a-chip technology. Based on the current work and gained knowledge from our current barrier formation optimization and toxicity studies a microfluidic multi-mucosa-on-a-chip platform is currently being developed. A main task still to be established within the project is a common ALI cultivation protocol and optimization of media supplements and growth factors that further improves the maturation of individual barrier properties. This step will allow the simultaneous integration of the four mucosa models within three to four weeks of on-chip maturation and maintenance. The combination of reliable mature barrier models [44] with fluid perfusion [45] and fluid shear stress [46] as well as gaseous particle-uptake [47,48] within an air-liquid-interface (i.e., using a nebulizer) can further uncover novel mechanisms and cellular processes needed to simulate both chronic and acute nanomaterial exposure scenarios. [49]

4. Materials and Methods

Cell lines and culture conditions. To replicate the pathway of inhaled toxicants, four key cell lines originating from the respiratory system were used:

- RPMI2650, (Sigma-Aldrich, Cat. Nr. 88031602) originating from squamous cell carcinoma of nasal epithelium, were cultured in EMEM (Sigma-Aldrich, Cat. Nr. M0325);
- A549 (ATCC, Cat. Nr. CCL-185) originating from adenocarcinoma from alveolar lung epithelium, were cultured in RPMI1640 (Sigma-Aldrich, Cat. Nr.R8758);
- TR146, (Sigma-Aldrich, Cat. Nr. 10032305) originating from squamous cell carcinoma of buccal (oral) epithelium, were cultured in Ham's F12 (Sigma-Aldrich, Cat. Nr. 51651C);
- Calu-3, (Sigma-Aldrich, Cat. Nr. HTB-55, kindly provided by IMC FH Krems) originating from adenocarcinoma from bronchial lung epithelium, were cultured in EMEM (Sigma-Aldrich, Cat. Nr. M0325).

All cell culture media were supplemented with 10% FBS (Sigma-Aldrich, Cat. Nr. F0804) and 1% Antibiotic- Antimycotic-solution (Sigma-Aldrich, Cat. Nr. A5955). Cells were kept in culture at humidified 37°C, 5% CO2, in TC-treated 75 cm2 flasks (Greiner Bio-One, Cat. Nr. 658175) and split twice a week, by trypsinization (0.5 g/L Trypsin – 0.2 g/L EDTA, Sigma-Aldrich, Cat. Nr. T3924).

 doi:10.20944/preprints202301.0445.v1

Growth properties and morphology were monitored during the cultivation of cells via light microscopy and counting with an improved Neubauer hemocytometer.

Barrier formation studies. Cells were seeded at 100% confluency, on thincerts (Greiner Bio-One, Cat. Nr. 665610, 3µm pore size and Cat. Nr. 665640) in a 12 well format (growth area: 1.12 cm2) that were coated with 0.12 mg/mL rat tail collagen I (Sigma-Aldrich, Cat. Nr. C3867) at 37°C for 1h. For this, different cell numbers were used for the four cell lines. RPMI2650: $1*10^6$ cells/thincert, A549: $5*10^5$ cells/thincert, TR146: $1*10^5$ cells/thincert, Calu-3: $5*10^5$ cells/thincert. The medium supplemented with 1 µM hydrocortisone (Sigma-Aldrich, Cat. Nr. H0888) was added to the cells 24 h post seeding. In the basal compartment 5.5 mL medium and in the apical compartment 0.5 mL medium was applied. On day 8 ALI was introduced, by removing the apical medium and reducing the basal medium to 4 mL. Medium was changed every 2-3 days, where also TEER was measured, using the EVOM3 (world precision instruments, wpi) combined with chopstick electrodes (STX3 and STX4, world precision instruments, wpi). Experiments were performed as triplicates (control LLI: n=3; 1µM hydrocortisone/HC LLI: n=3; blank n=1; control ALI: n=3; 1µM HC ALI: n=3). After 14 days at ALI (=d22 total) cells were fixed on thincerts ® for staining.

Evaluation of Tight junction formation via immunocytochemistry. After fixation with 4% paraformaldehyde (Sigma-Aldrich, Cat. Nr. P6148) and permeabilized with 0.2% Triton-X 100 (Sigma-Aldrich, Cat. Nr. X100) for 15 minutes. A 5% BSA (Sigma-Aldrich, Cat. Nr. A2153) was used as a blocking solution. Cells were then stained with 1 µg/mL Hoechst (Invitrogen, Cat. Nr. H1398), 1 unit/mL Phalloidin (Invitrogen, Cat. Nr. 21834), 5 µg/mL mouse-anti-ZO-1 monoclonal antibody (Invitrogen, Cat. Nr. 33-9100) and a 10 µg/mL goat anti-mouse IgG Alexa FluorTM 488 labeled secondary antibody (Invitrogen, Cat. Nr. A32723) to image cell-cell contacts and tight junction-associated proteins. All dyes and antibodies were diluted in PBS (Sigma-Aldrich, Cat. Nr. D8537) containing 0.5% BSA. Cells were washed three times for 5 minutes with PBS after blocking and in-between dying steps.

Toxicological evaluation of zinc oxide and titanium dioxide nanoparticles. Cells were seeded at 100% and 50% confluency on rat tail collagen I coated 96-well plates (Greiner Bio-One, Cat. Nr. 655101; growth area: 34 mm2). RPMI2650: $1.8*10^6$ and $9*10^4$ cells/well, A549: $1.2*10^5$ and $6*10^4$ cells/well, TR146: $3*10^4$ and $1.5*10^4$ cells/well, Calu-3: $6*10^4$ and $3*10^4$ cells/well. Nanoparticles, ZnO (Joint Research Centre, ID: NM62101a, 70-90 nm, uncoated), and TiO_2 (Joint Research Centre, ID: NM01001a, 5-6 nm, Anatase) were applied in different concentrations (0.125 - 2 mM) to the four cell lines. Untreated cells were used as a negative control. PrestoBlue™ Assay (Thermo Fisher Scientific, Cat. Nr. A13261) was used to measure cell viability. Medium in wells was removed and replaced with staining reagent, diluted 1:10 in medium and incubated for 3h. Read-out was performed via fluorescence measurements (Excitation: 560 nm; Emission: 590 nm) using an EnSpire 2300 plate reader by PerkinElmer. The same protocol was then applied for toxicology testing on the barrier models after 14 days of ALI on thincerts® and later on the chip model.

Supplementary Materials: The following supporting information can be downloaded at the website of this paper posted on Preprints.org, Figure S1: Comparison of conventional 2D monolayer cultures (100% confluent submerged) with mature barrier models grown 22 days under ALI cultivation protocols.

Author Contributions: H.S., E.I.R. and M.R. have contributed equally. Conceptualization, M.R., E.I.R., C.R., G.B. and G.P.; analysis and visualization, H.S. and M.R.; supervision, M.R. and E.I.R.; funding acquisition, M.R.; writing—original draft preparation, H.S., E.I.R and M.R.; writing—review and editing, H.S., E.I.R, M.P., H.H., P.E., W.N., C.R., G.B., G.P. and M.R. All authors have read and agreed to the published version of the manuscript.

Funding: This research was funded by the Austrian Ministry of Defense (BMLV).

Data Availability Statement: Data is available under reasonable email request.

Conflicts of Interest: The authors declare no conflict of interest.

References

1. De Matteis V. *Toxics*. 2017;5(4). doi:10.3390/TOXICS5040029
2. Lippmann M, Yeates DB, Albert RE. *Br J Ind Med*. 1980;37(4):337-362. doi:10.1136/oem.37.4.337
3. Morozesk M, Souza I da C, Fernandes MN, Soares DCF. *Environ Adv*. 2021;6:100125. doi:10.1016/j.envadv.2021.100125
4. Wang S, Alenius H, El-Nezami H, Karisola P. *Nanomaterials*. 2022;12(8). doi:10.3390/nano12081247
5. Xu L, Wang Y-Y, Huang J, Chen C-Y, Wang Z-X, Xie H. *Theranostics* . 2020;10:20. doi:10.7150/thno.45413
6. Majumder N, Goldsmith WT, Kodali VK, Velayutham M, Friend SA, Khramtsov V V, Nurkiewicz TR, Erdely A, Zeidler-Erdely PC, Castranova V, Harkema JR, Kelley EE, Hussain S. *Redox Biol*. 2021;46:102092. doi:10.1016/j.redox.2021.102092
7. García-Salvador A, Katsumiti A, Rojas E, Aristimuño C, Betanzos M, Martínez-Moro M, Moya SE, Goñi-De-cerio F. *Nanomaterials*. 2021;11(6). doi:10.3390/nano11061577
8. Giampaolo L Di, Zaccariello G, Benedetti A, Vecchiotti G, Caposano F, Sabbioni E, Groppi F, Manenti S, Niu Q, Maria A, Poma G, Gioacchino M Di, Petrarca C. 2021;11:270. doi:10.3390/nano11020270
9. Vandebriel RJ, De Jong WH. *Nanotechnol Sci Appl*. 2012;5(1):61. doi:10.2147/NSA.S23932
10. Castell J V, Donato MT, Gómez-Lechón MJ. *Exp Toxicol Pathol*. 2005;57(SUPPL. 1):189-204. doi:10.1016/J.ETP.2005.05.008
11. Hiemstra PS, Grootaers G, van der Does AM, Krul CAM, Kooter IM. *Toxicol Vitr*. 2018;47:137-146. doi:10.1016/j.tiv.2017.11.005
12. Seagrave JC, McDonald JD, Mauderly JL. *Exp Toxicol Pathol*. 2005;57(SUPPL. 1):233-238. doi:10.1016/j.etp.2005.05.011
13. Lenz AG, Karg E, Lentner B, Dittrich V, Brandenberger C, Rothen-Rutishauser B, Schulz H, Ferron GA, Schmid O. *Part Fibre Toxicol*. 2009;6:32. doi:10.1186/1743-8977-6-32
14. Ritter D, Knebel JW, Aufderheide M. *Exp Toxicol Pathol*. 2001;53(5):373-386. doi:10.1078/0940-2993-00204
15. Harkema JR, Carey SA, Wagner JG. *Toxicol Pathol*. 2006;34(3):252-269. doi:10.1080/01926230600713475
16. Squier CA, Kremer MJ. *J Natl Cancer Inst Monogr*. 2001;2001(29):7-15. doi:10.1093/oxfordjournals.jncimonographs.a003443
17. Fujino N, Kubo H, Suzuki T, Ota C, Hegab AE, He M, Suzuki S, Suzuki T, Yamada M, Kondo T, Kato H, Yamaya M. *Lab Investig*. 2011;91(3):363-378. doi:10.1038/LABINVEST.2010.187
18. Shen BQ, Finkbeiner WE, Wine JJ, Mrsny RJ, Widdicombe JH. *https://doi.org/101152/ajplung19942665L493*. 1994;266(5 10-5). doi:10.1152/AJPLUNG.1994.266.5.L493
19. Antonetti DA, Wolpert EB, DeMaio L, Harhaj NS, Scaduto RC. *J Neurochem*. 2002;80(4):667-677. doi:10.1046/j.0022-3042.2001.00740.x
20. Pozzoli M, Ong HX, Morgan L, Sukkar M, Traini D, Young PM, Sonvico F. *Eur J Pharm Biopharm*. 2016;107:223-233. doi:10.1016/j.ejpb.2016.07.010
21. Zhou P, Yang X Lou, Wang XG, et al. *Nature*. 2020;579(7798):270-273. doi:10.1038/s41586-020-2012-7
22. Ren H, Birch NP, Suresh V. *PLoS One*. 2016;11(10). doi:10.1371/journal.pone.0165225
23. Srivastava RK, Rahman Q, Kashyap MP, Singh AK, Jain G, Jahan S, Lohani M, Lantow M, Pant AB. *Hum Exp Toxicol*. 2013;32(2):153-166. doi:10.1177/0960327112462725
24. Chang Y, Yang ST, Liu JH, Dong E, Wang Y, Cao A, Liu Y, Wang H. *Toxicol Lett*. 2011;200(3):201-210. doi:10.1016/j.toxlet.2010.11.016
25. Blank F, Rothen-Rutishauser BM, Schurch S, Gehr P. *J Aerosol Med Depos Clear Eff Lung*. 2006;19(3):392-405. doi:10.1089/JAM.2006.19.392
26. Munis AM, Hyde SC, Gill DR. *Mol Ther - Methods Clin Dev*. 2021;20:237-246. doi:10.1016/j.omtm.2020.11.013
27. Mathias NR, Timoszyk J, Stetsko PI, Megill JR, Smith RL, Wall DA. *J Drug Target*. 2002;10(1):31-40. doi:10.1080/10611860290007504
28. Foster KA, Avery ML, Yazdanian M, Audus KL. *Int J Pharm*. 2000;208(1-2):1-11. doi:10.1016/S0378-5173(00)00452-X
29. Bol L, Galas JC, Hillaireau H, Le Potier I, Nicolas V, Haghiri-Gosnet AM, Fattal E, Taverna M. *Biomed Microdevices*. 2014;16(2):277-285. doi:10.1007/s10544-013-9831-3
30. Joy AP, Cowley EA. *Am J Respir Cell Mol Biol*. 2008;38(2):143-152. doi:10.1165/rcmb.2006-0295OC
31. Min KA, Rosania GR, Kim CK, Shin MC. *Arch Pharm Res*. 2016;39(3):359-369. doi:10.1007/s12272-015-0704-6
32. Reichl S, Becker K. *J Pharm Pharmacol*. 2012;64(11):1621-1630. doi:10.1111/j.2042-7158.2012.01540.x
33. Wengst A, Reichl S. *Eur J Pharm Biopharm*. 2010;74(2):290-297. doi:10.1016/j.ejpb.2009.08.008
34. Kreft ME, Jerman UD, Lasič E, Rižner TL, Hevir-Kene N, Peternel L, Kristan K. *Pharm Res*. 2015;32(2):665-679. doi:10.1007/s11095-014-1494-0
35. Lin GC, Leitgeb T, Vladetic A, Friedl HP, Rhodes N, Rossi A, Roblegg E, Neuhaus W. *Tissue Barriers*. Published online 2020. doi:10.1080/21688370.2020.1748459
36. Jacobsen J, Nielsen EB, Brøndum-Nielsen K, Christensen ME, Olin HD, Tommerup N, Rassing MR. *Eur J Oral Sci*. 1999;107(2):138-146. doi:10.1046/j.0909-8836.1999.eos107210.x

37. Braakhuis HM, He R, Vandebriel RJ, Gremmer ER, Zwart E, Vermeulen JP, Fokkens P, Boere J, Gosens I, Cassee FR. *J Vis Exp*. 2020;2020(159). doi:10.3791/61210
38. Barosova H, Meldrum K, Karakocak BB, Balog S, Doak SH, Petri-Fink A, Clift MJD, Rothen-Rutishauser B. *Toxicol Vitr*. 2021;75:105178. doi:10.1016/j.tiv.2021.105178
39. Heng BC, Zhao X, Xiong S, Ng KW, Boey FYC, Loo JSC. *Arch Toxicol*. 2011;85(6):695-704. doi:10.1007/s00204-010-0608-7
40. Leroux MM, Doumandji Z, Chézeau L, Gaté L, Nahle S, Hocquel R, Zhernovkov V, Migot S, Ghanbaja J, Bonnet C, Schneider R, Rihn BH, Ferrari L, Joubert O. *Int J Mol Sci*. 2020;21(14):1-23. doi:10.3390/ijms21144855
41. Wang M, Yang Q, Long J, Ding Y, Zou X, Liao G, Cao Y. *Int J Nanomedicine*. 2018;13:8037-8049. doi:10.2147/IJN.S188175
42. Čepin M, Hribar G, Caserman S, Orel ZC. *Mater Sci Eng C*. 2015;52:204-211. doi:10.1016/J.MSEC.2015.03.053
43. He T, Long J, Li J, Liu L, Cao Y. *Environ Toxicol Pharmacol*. 2017;56:233-240. doi:10.1016/j.etap.2017.10.002
44. Sticker D, Rothbauer M, Lechner S, Hehenberger MT, Ertl P. *Lab Chip*. 2015;15(24):4542-4554. doi:10.1039/c5lc01028d
45. Schuller P, Rothbauer M, Kratz SRA, Höll G, Taus P, Schinnerl M, Genser J, Bastus N, Moriones OH, Puntes V, Huppertz B, Siwetz M, Wanzenböck H, Ertl P. *Sensors Actuators B Chem*. 2020;312:127946. doi:10.1016/J.SNB.2020.127946
46. Charwat V, Olmos Calvo I, Rothbauer M, Kratz SRA, Jungreuthmayer C, Zanghellini J, Grillari J, Ertl P. *Anal Chem*. 2018;90(6):3651-3655. doi:10.1021/acs.analchem.7b04788
47. Guénette J, Breznan D, Thomson EM. *Inhal Toxicol*. 2022;34(3-4):80-89. doi:10.1080/08958378.2022.2039332/SUPPL_FILE/IIHT_A_2039332_SM0122.JPG
48. Binder S, Rastak N, Karg E, Huber A, Kuhn E, Dragan GC, Monsé C, Breuer D, Di Bucchianico S, Delaval MN, Oeder S, Sklorz M, Zimmermann R. *Toxics 2022, Vol 10, Page 730*. 2022;10(12):730. doi:10.3390/TOXICS10120730
49. Rothbauer M, Praisler I, Docter D, Stauber RH, Ertl P. *Biosens 2015, Vol 5, Pages 736-749*. 2015;5(4):736-749. doi:10.3390/BIOS5040736